RSC Advances

ROYAL SOCIETY OF CHEMISTRY

www.rsc.org/advances

RSC Advances

RSC Publishing

Paper

Modification of Fe_3O_4 Superparamagnetic Nanoparticles with Zirconium Oxide; Preparation, Characterization and its Application toward Fluoride Removal

Cite this: DOI: 10.1039/xoxxoooooox

Received ooth January 2012,
Accepted ooth January 2012

DOI: 10.1039/xoxxoooooox

www.rsc.org/

F. Riahi[a], M. Bagherzadeh[*a] and Z. Hadizadeh[b]

Fe_3O_4 superparamagnetic nanoparticles (NPs) modified with zirconia (ZrO_2) were synthesized (Fe_3O_4@ZrO_2) using a chemical co-precipitation method and used as nanoadsorbent in removal excessive fluoride from aqueous solutions. This adsorbent combines the advantages of magnetic nanomaterial and F^- sorbent floc, with magnetic separability and high affinity toward fluoride, which provides distinctive merits including easy preparation, high adsorption capacity, and easy isolation from sample solutions by the application of an external magnetic field. The prepared Fe_3O_4@ZrO_2 magnetic nanoparticles were characterized by XPS, XRD, SEM, EDXA, BET, FTIR, and VSM techniques. Affecting parameters on removal of fluoride, such as mass ratio of Fe_3O_4 to ZrO_2, solution pH, adsorption time, initial fluoride concentration, and co-existing anions were investigated. The high adsorption capacity calculated by Langmuir equation was 158.6 mg g^{-1} for Fe_3O_4@ZrO_2 (2:5) in pH 2.5. The adsorption capacity increased with temperature and the kinetics followed a pseudo-second-order rate equation. The enthalpy change (ΔH^0) and entropy change (ΔS^0) was 25.02 kJ mol^{-1} and 3.76 J mol^{-1} K^{-1}, which substantiates the endothermic and spontaneous nature of the fluoride adsorption process. Furthermore, the residual concentration of fluoride using Fe_3O_4@ZrO_2 NPs as adsorbent could reach 0.3 mg L^{-1} with an initial concentration of 20 mg L^{-1}. Also application of Fe_3O_4@ZrO_2 NPs for removal of fluoride from real samples was tested. All of the results suggested that the Fe_3O_4@ZrO_2 NPs with strong and specific affinity toward fluoride could be excellent adsorbent for treatment of fluoride contaminated water.

1. Introduction

Nanoscience is one of the most important research and development frontiers in modern science. The use of nanoparticles (NPs) materials offers many advantages due to their unique size and physical properties [1]. Magnetic nanoparticles (MNPs) are of great interest for researchers from a wide range of disciplines, including magnetic fluids, catalysis, biotechnology/biomedicine, magnetic resonance imaging, data storage, and environmental remediation [2]. Magnetic materials, such as superparamagnetic iron oxide (SPIO) particles, have been extensively used for the removal of heavy metal ions, organic dyes and herbicides from aqueous media [3-6]. Additionally, magnetic materials are the most commonly selected substrates as affinity probes because of the ease of isolation of the magnetic-material-target conjugate from the sample solutions based on their magnetic properties [7]. Affinity probes with magnetic properties lead the isolation of the trapped species from sample solutions very conveniently and rapidly; therefore, the time required for separation can be dramatically reduced.

In a typical procedure for separation, firstly the SPIOs must be modified by suitable modifier, and after that interact with target molecule or ion, subsequently will be separated by an external magnetic field. Modification of the SPIO surface has been successfully done by using carbon, organic polymers, surfactants, silica, precious metals, and metal oxides. These modifications not only cause to selective separation but also to preserve their specific magnetic properties, and protect nanoparticles from both oxidation and agglomeration [1].

Metal oxides such as titania [8], alumina [9], and zirconia (ZrO_2) [10] have been demonstrated to be effective materials for the selective separation of anions from aqueous solutions. It has been reported that La(III), Ce(IV), Y(III), and Zr(IV) oxides had high adsorption capacity for fluoride [11,12]. Among these adsorbents, zirconium-based materials have been paid more attention in recent investigations due to their high binding affinity with fluoride [13]. Recently, Chen et al. and Zhang et al. synthesized ZrO_2 coated magnetic particles, and used them as the trapping adsorbents for the analysis of phosphopeptides [14,15]. The ZrO_2 coated magnetic particles that they were synthesized, didn't show superparamagnetic behaviour and have been employed for enrichment and separation of phosphopeptides. Although, there are a few reports on strong attraction between ZrO_2 and fluoride in literature, but there is not report about enrichment and separation of fluoride, especially in pollution cases, by using magnetized ZrO_2.

Fluoride contamination in the drinking water due to natural reasons and human activities is a major problem worldwide [16]. According to World Health Organization (WHO) norms, the upper limit of fluoride in drinking water is 1.5 mgL^{-1} [17]. Several methods have been applied to remove excessive fluoride, such as precipitation [18], ion-exchange [19], and adsorption [20]. Adsorption seems to be the most attractive method for the removal of fluoride below 1 mgL^{-1}. Because of large surface areas, it is likely that nanosized adsorbents can be a useful tool in enhancing the adsorption capacity in drinking water treatment. Unfortunately, ultra-fine particles cannot be applied in usual packed bed reactors and solid/liquid separation in completely stirred tank reactors is difficult or impossible. Magnetic adsorbents overcome the shortcoming of nonmagnetic nanomaterials and are very promising for application in the field of pre-concentration and removal pollutants [21].

Here, a simple defluoridation method, based on magnetic carrier technology and nanoadsorbent, established. Firstly, $Fe_3O_4@ZrO_2$ NPs were successfully synthesized via co-precipitation method, and characterized. Affecting parameters on removal of fluoride, such as mass ratio of Fe_3O_4 to ZrO_2, solution pH, adsorption time, initial fluoride concentration, and co-existing anions were investigated. Finally, application of $Fe_3O_4@ZrO_2$ NPs in fluoride removal from tap and river water samples, with 3 different levels of fluoride content, was studied. The data are presented and discussed here.

2. Experimental

2.1. Chemicals and materials

All reagents were of analytical reagent-grade and were used as supplied. Zirconium chloride ($ZrCl_4$), ferric chloride ($FeCl_3 \cdot 6H_2O$), ferrous chloride ($FeCl_2 \cdot 4H_2O$) and sodium fluoride (NaF, analytical reagent (AR) grade) were purchased from Merck®. Eriochrome cyanine R and zirconylchloride octahydrate, which was used for fluoride determination, also were provided from Merck®. Standard stock solutions of fluoride (1000 mgL^{-1} or 52 mmol L^{-1} F^-) were prepared by dissolving 0.221 g sodium fluoride into 100 mL deionized water and stored under dark conditions at 4 °C. All solutions were prepared with purified water (18 MΩ cm, Millipore-MilliQ, Millipore Inc.). All other chemicals used were either analytical or reagent grade.

2.2. Preparation of Fe_3O_4 nanoparticles

The Fe_3O_4 nanoparticles were prepared by chemical co-precipitation methods [22]. Briefly, 5.2 g of $FeCl_3 \cdot 6H_2O$, 2.0 g of $FeCl_2 \cdot 4H_2O$ were dissolved in 25 mL 1 M of HCl (degassed with nitrogen gas before use for 20 minutes). Then, the solution was added drop wise into 250 mL of 1.5 M NaOH solution under vigorous stirring using magnetic stirrer at 80 °C. The obtained Fe_3O_4 nanoparticles were separated from the reaction medium by magnetic field, and washed with 200 mL deionized water four times, then resuspended in 100mL deionized water and used for next section.

2.3. Preparation of $Fe_3O_4@ZrO_2$ nanoparticles

The $Fe_3O_4@ZrO_2$ nanoparticles were synthesized based on previous reported metal oxide preparation method [23]. For preparation of zirconium (IV) solutions, in which zirconium ion exists in its monomeric non-hydrolyzed form (i.e. solvated Zr^{4+}), first a small amount of the solid zirconium tetrachloride was weighed and dissolved in concentrated perchloric acid ($HClO_4$) [24], and then, diluted carefully with water to give a solution, which was 1.0 M in Zr(IV) and 0.23 M in $HClO_4$. Freshly prepared solution was added drop wise into the Fe_3O_4 NPs suspension and the pH value of the mixture was adjusted to 8.0 by addition of 2 M NaOH within 1 h. The mixture stirred for 2 h after the addition. During the whole process, temperature maintained at 80 °C and nitrogen gas used to prevent the intrusion of oxygen. The mass ratio of Fe_3O_4 to ZrO_2 was 2:2, 2:3, 2:5, and 2:7 by varying the proportion of ZrO_2 to suspended Fe_3O_4 NPs and the resulted particles specified as $Fe_3O_4@ZrO_2$ (2:2), $Fe_3O_4@ZrO_2$ (2:3), $Fe_3O_4@ZrO_2$ (2:5) and $Fe_3O_4@ZrO_2$ (2:7), respectively. Finally, the formed NPs thoroughly washed with deionized water and resuspended in deionized water. The concentration of the generated nanoparticles suspension estimated to be about 20 mg mL^{-1} ($Fe_3O_4@ZrO_2$ (2:5)).

2.4. Apparatuses and methods

The X-ray photoelectron spectroscopy (XPS) instrument was equipped with a hemispherical analyzer along with data acquisition system, and an AlK_α X-ray source (hv=1486.6 eV) operating at pressure lower than 10^{-10} Pa. The XPS peaks were fitted by Gaussian components model after a Shirley background subtraction. The X-ray diffraction patterns (XRD) and the crystal structure of pure synthetic Fe_3O_4 and $Fe_3O_4@ZrO_2$ (2:5) MNPs were obtained by an X-ray diffractometer (XRD, Bruker Advanced D8 model), using CuK_α radiation (λ=1.5406 A°). Morphology and elemental analysis of the samples determined by scanning electron microscope (SEM) equipped with EDXA (Philips XL-30). The size of the as-prepared particles was characterized using transmission electron microscope, TEM, (Philips-EM-208S). Magnetic properties were analyzed using a vibrating sample magnetometer (VSM, Daghigh Meghnatis Kashan Co., Kashan, Iran). Fourier-transform infrared (FTIR) spectroscopy analysis was performed with a Nicolet Impact 400D Model spectrophotometer (Nicolet Impact, Madison, USA). The surface charge of the nanoparticles was investigated on Malvern Zetasizer Nano ZS 90 zeta potential analyzer (Westborough, MA, USA). The specific surface areas of adsorbents were determined by the BET method with N_2 gas. Electrochemical measurements were performed on a Metrohm 797VA (Herisau, Switzerland). A surface modified carbon paste, as a working electrode, a Pt wire as a counter electrode, and an Ag/AgCl as a reference electrode were used. UV-Vis spectrophotometer (CINTRA 404) was used for fluoride determination. The concentration of fluoride ion was diluted to range of 0 to 50 µg in 50 ml before spectrophotometric analysis.

2.5. Batch adsorption experiments

Before adsorption experiments, standard stock solutions of fluoride (1000 mg L^{-1} F) were prepared and stored under dark conditions at 4 °C. Fluoride-bearing solutions were prepared by diluting the stock solution to given concentrations with deionized water. The fluoride concentration in aqueous solutions was measured by an ultraviolet-visible (UV-Vis) spectrophotometer. This method allowed determination of fluoride concentrations in the range of 0.1 to 1.0 mg L^{-1} [25]. The method required calibration curves prepared from decreasing in absorption intensity of reagents in 531 nm during addition of the standard sodium fluoride solutions (0.1– 1.0 mg L^{-1}) (see the supplementary material, Fig. S1). For selection of the best absorbent, 20 mg of $Fe_3O_4@ZrO_2$ NPs with different mass ratios of Fe_3O_4 to ZrO_2 (2:2, 2:3, 2:5, and 2:7) were thoroughly mixed with 50 mL of a 50 mg L^{-1} fluoride solution for 60 min. The effect of pH on the fluoride adsorption was investigated using an initial fluoride concentration of 50 mg/L, with 20 mg of adsorbent and a total suspension volume of 50 mL. Kinetics experiments were carried out at room temperature. The $Fe_3O_4@ZrO_2$ MNPs of 50 mg were immersed in 50 mL fluoride solutions with the initial fluoride concentrations of 25 and 50 mg L^{-1}, respectively. The mixtures were shaken at 150 rpm and approximately 0.5 mL aliquots were taken from the suspension at predetermined times and quickly separated by a permanent magnet. The adsorption isotherms were studied with a sorbent loading of 1 g L^{-1} at pH 2.5. Typically, 50 mg $Fe_3O_4@ZrO_2$ MNPs was added to 50 mL fluoride solutions of varying initial concentrations (10, 25, 50, 100, 150, and 200 mg L^{-1}).

RSC Advances

RSC Publishing

Paper

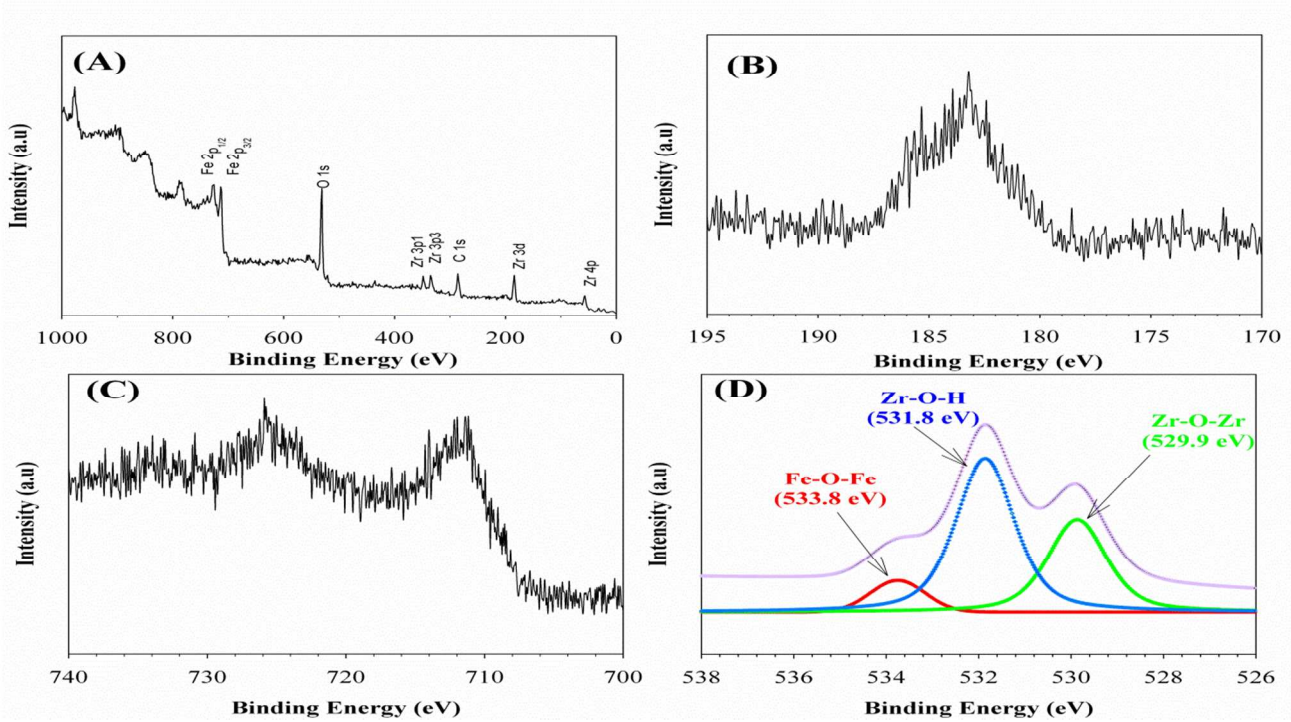

Fig. 1. XPS spectrum of the precipitated ZrO_2 on Fe_3O_4: (a) XPS survey spectrum; (b) XPS spectrum of Zr 3d; (c) XPS spectrum of Fe 2p and (d) deconvolution result of XPS O 1s core-level spectra..

The solutions were oscillated at 150 rpm for 50 min to achieve equilibrium, and then separated by a permanent magnet.

The residual fluoride concentration in solution was measured by the UV-Vis spectrophotometer. The adsorption capacity at equilibrium was calculated according to the following equation:

$$q_e = \frac{(C_0 - C_e)V}{m}$$

where C_o and C_e represent the initial and equilibrium fluoride concentrations (mg L^{-1}) respectively, V is the volume of the fluoride solution (mL), and m is the amount of adsorbent (g).

The effects of co-existing anions (nitrate, sulfate, chloride, bicarbonate) on fluoride adsorption were performed with an adsorbent dose of 1 g L^{-1} and an initial fluoride concentration of 50 mg L^{-1} at pH 2.5. Application of Fe_3O_4@ZrO_2 MNPs in real samples, was carried out with an adsorbent dose of 0.25 g L^{-1} in 500 ml tap water containing 1, 5, 10 mg L^{-1} of fluoride ion.

3. Results and discussion

3.1. Characterization of Fe_3O_4@ZrO_2 nanoparticles

The chemical composition and corresponding chemical state of the as-prepared Fe_3O_4@ZrO_2 particles were investigated by XPS. As shown in Fig. 1A, peaks corresponding to zirconium (Zr), oxygen (O), carbon (C), and iron (Fe) elements are clearly recognized on the survey spectrum, indicating that the as-prepared Fe_3O_4@ZrO_2 particles are consisted of iron and zirconium-related substances. As depicted in Fig. 1B, the binding energies for Zr 3d 5/2 and Zr 3d 3/2 are around 183.0 eV, which can be identified as Zr(IV) in the oxide [26,27]. Also as can be seen in Fig. 1C, the binding energies for Fe 2p 3/2 and Fe 2p 1/2 are 711.9 and 725.9 eV, respectively, which correspond to the XPS spectrum of Fe_3O_4 [28]. Deconvolution of O1s core-level spectrum results in three components: Zr–O–Zr (529.9 eV), Zr–O–H (531.8 eV) [29,30], and Fe–O–Fe (533.8 eV) [28], as clearly displayed in Fig. 1D. Anyway, XPS results support formation of zirconia on the Fe_3O_4.

The XRD patterns of the as-prepared Fe_3O_4@ZrO_2 (a) and Fe_3O_4 (b) particles are shown in Fig. 2A. Comparison of the XRD patterns of the pure sample Fe_3O_4 and Fe_3O_4@ZrO_2 (2:5) MNPs clearly revealed the existence of zirconia in the resulting particles. As shown in pattern (a) of Fig. 2A, the diffraction peaks at d-values of $2\theta = 30.4^{\circ}$, 35.2, 50.6, and 60.3° were indexed to (111), (200), (220), and (311) planes of zirconium oxide, respectively. It is also, the diffraction peaks at d-values of $2\theta = 30.0^{\circ}$, 35.5, 57.2, 62.7, and 89.9° were indexed to (220), (311), (511), (440), and (731) planes of magnetite, in which demonstrated no impurity peaks are detected and the high purity Fe_3O_4 spinel structure is synthesized (pattern (b)).The mean crystallite size of the powders was calculated from the broadening of XRD peaks (pattern (b)), using Scherrer's formula [31] as 12±1 nm.

The morphology and elemental structure of as-prepared Fe_3O_4@ZrO_2 particles were further examined by SEM and EDXA, (Fig. 2B, and C respectively). As can be seen from the SEM image (Figure 2B), morphology of bulk Fe_3O_4@ZrO_2 particles is irregular but their distribution is uniform. The energy dispersive X-ray

RSC Advances RSC Publishing

Paper

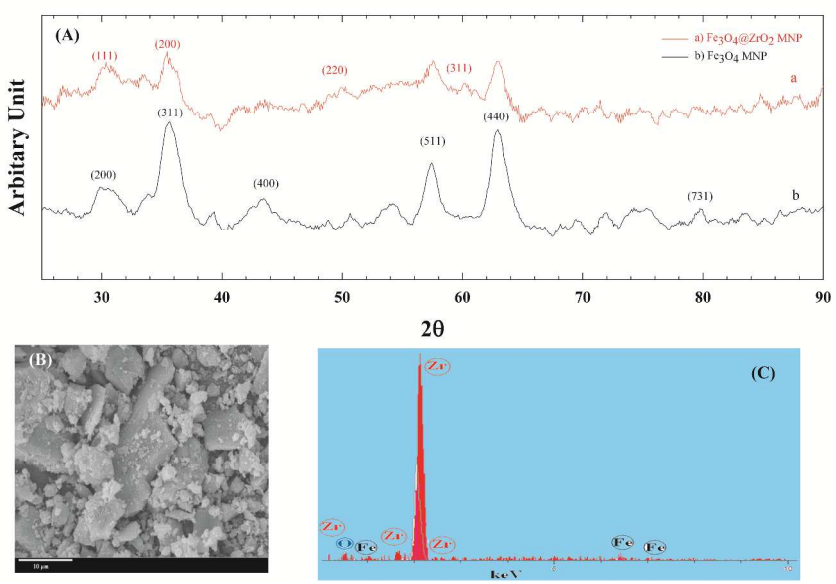

Fig. 2. Typical **(A)** XRD of as-prepared Fe_3O_4@ZrO_2 (2:5) (a) and Fe_3O_4 (b), **(B)** SEM image and EDXA **(C)** of as-prepared Fe_3O_4@ZrO_2 particles. The scale bar in SEM image is 10 µm.

analysis (Figure 1C) of the obtained Fe_3O_4@ZrO_2 by illuminating electron beams on the obtained core-shell microspheres reveals the existence of Fe, Zr, and O elements, furthermore confirming the formation of zirconia on the Fe_3O_4.

Fig. 3A and B shows the typical TEM images of as-prepared Fe_3O_4@ZrO_2 nanoparticles. As displayed, the particles exhibited spherical morphology but with small tendency to agglomeration.

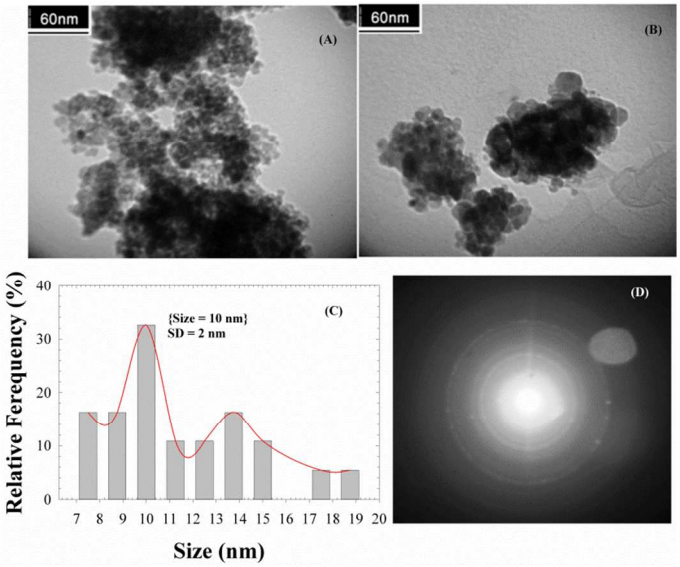

Fig. 3. Typical TEM images (A) and (B), particle size distribution (C), and SAED (D) image of Fe_3O_4@ZrO_2 (2:5) nanoparticles. The scale bar in TEM images (A) and (B) 60 nm.

In general, magnetite nanoparticles synthesized through the co-precipitation are usually agglomerate, that to achieve stable colloids, avoid agglomeration, the surface of magnetite nanoparticles precipitate can be modified by desired organic or inorganic modifiers. However, from TEM image, the average size of dispersed Fe_3O_4@ZrO_2 particles was estimated about 10 nm (Fig 3C). Moreover, the zeta potential of suspension for Fe_3O_4@ZrO_2 particles was −34.1 (± 0.2) mV (see the supplementary material, Fig. S2) which was smaller than that of Fe_3O_4 NPs considering that zirconia modification protect the Fe_3O_4 NPs away from aggregation. SAED image obtained from the edge and the center of one of the spherical, non-agglomerated Fe_3O_4@ZrO_2 particle, is shown in Fig 3D.

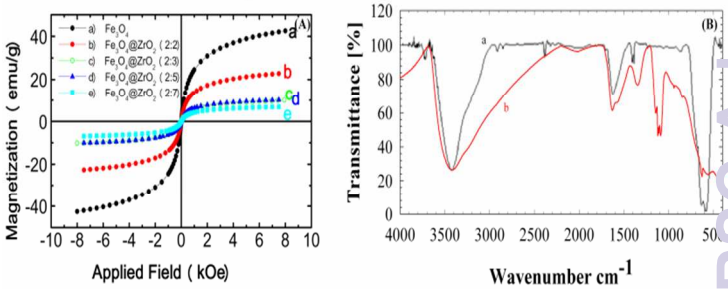

Fig. 4. Typical VSM **(A)** of as-prepared Fe_3O_4 (a), Fe_3O_4@ZrO_2 (2:2) (b), Fe_3O_4@ZrO_2 (2:3) (c), Fe_3O_4@ZrO_2 (2:5) (d), and Fe_3O_4@ZrO_2 (2:7) (e), and typical FTIR spectrum **(B)** of as-prepared Fe_3O_4 (a) and Fe_3O_4@ZrO_2 (2:5) (b).

Table 1. The values of saturation magnetization (M_s), remanent magnetization (M_r) and coercivity (H_c) of Fe_3O_4, Fe_3O_4@ZrO_2 (2:2), Fe_3O_4@ZrO_2 (2:3), Fe_3O_4@ZrO_2 (2:5) and Fe_3O_4@ZrO_2 (2:7) MNPs, extracted from Fig. 2A.

Type of MNP	M_s/(emu g^{-1})	M_r/(emu g^{-1})	H_C/Oe
Fe_3O_4	42.55	0.02≈0	2.2
Fe_3O_4@ZrO_2 (2:2)	22.76	0.01≈0	1.5
Fe_3O_4@ZrO_2 (2:3)	10.13	0.02≈0	0.8
Fe_3O_4@ZrO_2 (2:5)	10.04	0.01≈0	0.9
Fe_3O_4@ZrO_2 (2:7)	6.89	0.01≈0	1.0

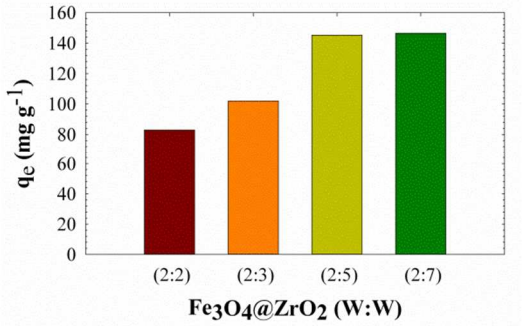

Fig. 5. Effect of Fe_3O_4@ZrO_2 mass ratio on fluoride removal, performed with initial concentration of 50 mg L^{-1}, pH 2.5 and 25°C.

A number of diffraction spots are observed in the SAED pattern obtained from the edge of the Fe_3O_4@ZrO_2 particle. As can be seen there are diffraction spots when traversed from the edge towards the center of the particle. This indicates that a large number of nanocrystallites are located at the edge of the particle than that at the particle center. The TEM images and corresponding SAED, XRD patterns, EDXA, and XPS spectrum, strongly suggest that the spherical, ZrO_2 particles are made up of large number of small-sized tetragonal Fe_3O_4 nanocrystallites.

Maximum magnetic strength for MNP, is an important characteristic for magnetic separation and MNPs synthesized here possess superparamagnetic behaviour with strong magnetic power. Fig. 4A shows the VSM magnetization curves of Fe_3O_4 and Fe_3O_4@ZrO_2 MNPs with different mass ratio of ZrO_2. Because of shielding effect of ZrO_2 NPs, with the increase in the mass ratio of ZrO_2, a decrease occurred in the magnetic strength of the MNPs. In the sequence of Fe_3O_4, Fe_3O_4@ZrO_2 (2:2), Fe_3O_4@ZrO_2 (2:3), Fe_3O_4@ZrO_2 (2:5) and Fe_3O_4@ZrO_2 (2:7), the saturation magnetization were 42.55, 22.76, 10.13, 10.04, and 6.89 emu g^{-1}, respectively. The saturation magnetization of 10.13 emu g^{-1} for the Fe_3O_4@ZrO_2 (2:5) was high enough for magnetic separation. The results proved the magnetic nanoparticles exhibited typical superparamagnetic behaviour, characterized with strong magnetic susceptibility and no hysteresis, remanence and coercivity (Table 1). These results verified the successful synthesize of Fe_3O_4@ZrO_2 magnetic nanoparticles and superparamagnetic behaviour of them. Finally, the specific surface area of Fe_3O_4@ZrO_2 MNP (2:5) was determined by BET method to be 492 m^2 g^{-1}.

To further prove successful preparation of Fe_3O_4@ZrO_2 NPs, the FT-IR spectroscopy was employed to examine the surfaces of the as-made Fe_3O_4 and Fe_3O_4@ZrO_2 NPs. The characteristic band of Fe_3O_4 appears at ~576 cm^{-1} (Fig. 4B spectrum a) [32]. The FT-IR spectrum of the Fe_3O_4@ZrO_2 NPs (Fig. 4B spectrum b) shows characteristic bands at 634 cm^{-1}, which is due to the Zr-O bond of zirconia [33]. Hence, these FT-IR spectroscopy results provide additional evidence for successful synthesis of Fe_3O_4@ZrO_2 NPs. The results support presence of ZrO_2 on the surface of magnetic nanoparticles, and thus, modifications took place on the Fe_3O_4 NPs, i.e. the resulted Fe_3O_4@ZrO_2 MNPs have unique behaviours of zirconium oxide in addition to magnetic property.

3.2. Interaction of Fe_3O_4@ZrO_2 MNPs with fluoride

Affinity of prepared Fe_3O_4@ZrO_2 MNPs with different mass ratio of ZrO_2 toward fluoride was examined and presented in Fig. 5. As can be seen with the increasing in the mass ratio of ZrO_2 in the Fe_3O_4@ZrO_2 series, fluoride adsorption capability of MNPs increased remarkably. In the sequence of Fe_3O_4@ZrO_2 (2:2), Fe_3O_4@ZrO_2 (2:3), Fe_3O_4@ZrO_2 (2:5) and Fe_3O_4@ZrO_2 (2:7), the adsorptions of fluoride were 83.0, 102.0, 145.2 and 146.5 mg g^{-1}, respectively.

Thus, Fe_3O_4@ZrO_2 (2:5) MNPs because of high adsorption capacity and strong magnetic property (Fig. 4A) were selected for further adsorption experiments and magnetic separation tests.

3.3. Effect of solution pH on fluoride removal

Generally, a main factor determining the fluoride loading onto the adsorbents surface is the charge density that varies strongly with pH, and fluoride adsorption on Fe_3O_4@ZrO_2 surface is therefore dependent on the initial solution pH. The influence of the pH values on fluoride removal by the Fe_3O_4@ZrO_2 MNPs with various initial concentrations was investigated, and the results are shown in Fig. 6. It is clear that the optimum pH for the fluoride adsorption was in the pH 2.5. Thus, the kinetic and isotherm experiments were carried out at pH 2.5 in this study (section 3.6). At pH 2.5, with initial fluoride concentrations of 50 mg L^{-1}, the equilibrium adsorption capacity was 123.9 mg g^{-1}. Furthermore, the adsorption capacities were decreased step by step with the increased pH values, as shown in Fig. 6, which might be due to the changes of pH-dependent electrostatic attraction between the adsorbent surface and fluoride. So, the influence of the pH value on the surface potential was investigated, and the results are shown in Fig. 7. Generally, the surface functional groups have deferent charges in certain pHs that simplicity can probe by electrochemical methods [34] and from which can estimate surface pK_a of end functional groups of surface nanoparticles. In this part of the present work, we have estimated the surface pKa of the Fe_3O_4@ZrO_2 MNP by faradaic current titration, as an almost straightforward method, and then, verified the validity of our findings by comparison with pH of the point of zero charge (pH_{PZC}) value which obtained in the previous work. The surface pKa of the

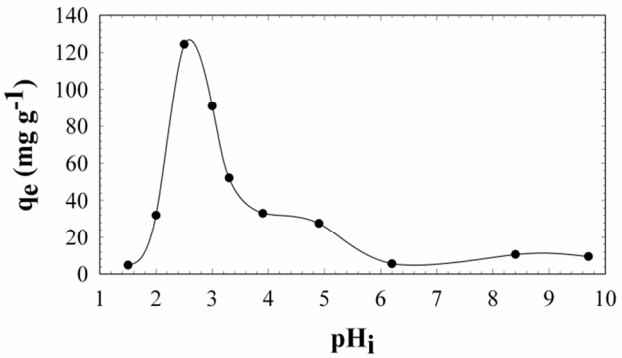

Fig. 6. Effect of pH on the removal of fluoride by Fe_3O_4@ZrO_2 MNPs with initial fluoride concentrations of 50 mg L^{-1}, adsorbent dose 1 mg mL^{-1}, 25 °C and contact time 24 h.

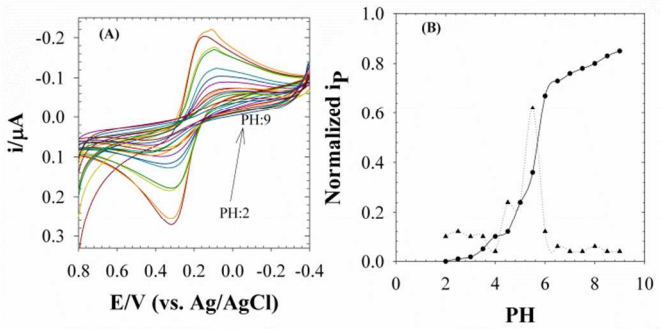

Fig. 7. **(A)** Cyclic voltammograms obtained for a carbon paste electrode modified by Fe_3O_4@ZrO_2 MNPs in phosphate buffer solution containing 0.1 M $NaClO_4$ in the presence of 0.5 mM $Fe(CN)_6]^{3-/4-}$, scan rate: 100 mV s^{-1}. Outer to inner; pH 2.0, 2.5, 3.0, 3.5, 4.0, 4.5, 5.0, 5.5, 6.0, 6.5, 7.0, 7.5, 8.0, 8.5 and 9.0. **(B)** Reversible variation of i_p extracted from cyclic voltammograms for modified electrode, normalized i_p is $(i_{p(max)} - i_p)/i_{p(max)}$.

Fe_3O_4@ZrO_2 MNP were estimated by recording the cyclic voltammograms of a modified carbon paste electrode by Fe_3O_4@ZrO_2 MNP in a wide range of pH (Fig. 7A), and then, monitoring of i_p as functions of pH. Value of 5.5±0.1 was obtained from midpoint of the titration curve for Fe_3O_4@ZrO_2 (Fig. 7B). This value is in good agreement with pH_{PZC} as 5.8 reported by Chang et al. [35]. Finally, the Fe_3O_4@ZrO_2 MNPs have a pKa at about pH 5.5, suggesting that the adsorbent surface has positive charge at pHs below 5.5. As a result, the low pH value is favourable for fluoride ions removal owing to the electrostatic attraction. On the contrary, when the pH value is up to and larger than 5.5, the adsorbent surface became negatively charged. The higher pH means the more negative surface, which will result in the strong electrostatic repulsion between adsorbent and the fluoride ions, as well as the clearly decreased adsorption capacities, as shown in Fig. 6. In addition, in spite of the pKa, the adsorption capacities were also decreased with the decreasing the pH from 2.5 to 1.5. This might be due to the formation of hydrofluoric acid, which results in lower available fluoride concentration than the actual concentration for adsorption on the adsorbent. Because of strong acidity was appropriate for the handling of industrial wastewater, acidic solution (pH 2.5) was selected for subsequent experiments. Acidic initial pH was helpful for fluoride adsorption, which agreed well with the possible adsorption mechanism. It is important to mention here that the optimized pH range of 2.0-3.0 indicates the potential application of developed adsorbent for industrial waste water systems.

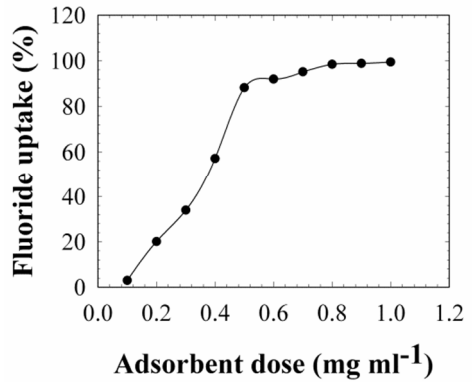

Fig. 8. Effect of sorbent dosage on the uptake of fluoride, pH 2.5, 25 °C and contact time 24 h.

It should be mentioned that the adsorption capacities were dramatically decreased and reduced to almost zero when the pH value reached to 10. The results were consistent with the ones of other metal impregnated adsorbents [36-38]. The decreasing in fluoride adsorption in the alkaline pH range may be due to the competition from OH^- ions present in the sample solution with fluoride ion for replacement in the sorption site. So, the high pH value was benefit to desorption of fluoride from the adsorbent. We could take this experimental phenomenon as an approach for desorption of fluoride from the adsorbent.

3.4. Optimization of sorbent dosage.

Studying the effect of the sorbent dosage gives an idea of the effectiveness of a sorbent. Herein, the sorption of fluoride using the Fe_3O_4@ZrO_2 MNP has been analyzed by varying the sorbent dosage in the range 5-50 mg. The removal percentage of fluoride with different dosages of sorbent is shown in Fig. 8. Initially, the percentage removal increased with an increase in the dosage and then it remained almost constant on further increasing the sorbent dose. The increase in the number of active adsorption sites of the sorbent with increasing the doses, explains the initial increase in the uptake percentage. At a sorbent dose of 0.25 mg the uptake became constant because the amount of available sites on the composite is more than needed for a fixed amount of fluoride (50 mg L^{-1}). To ensure the complete removal of fluoride from the solution, 0.50 mg of sorbent (1 mg mL^{-1}) was fixed as an optimum dosage of sorbent for the rest of the experiments.

3.5. Adsorption isotherm

The defluoridation method using Fe_3O_4@ZrO_2 MNPs as adsorbents allowed rapid removal of fluoride by a simple magnetic field extraction method. Equilibrium isotherm experiments were conducted on the synthetic sample solutions with initial fluoride concentrations ranging in 5–150 mgL^{-1} using batch procedure at 25±1 °C and its effect showed in Fig. 9. Equilibrium experiments were carried out at 25±1 °C in water bath with vigorous stirring using a non magnetic stirrer under 1 h. Each time 50 mg of Fe_3O_4@ZrO_2 MNPs suspension was added into 50 mL of sample solutions containing fluoride ion and placed in an inert 100 mL polyethylene beaker. The initial pH of the sample solution was adjusted to the value of 2.5 with 0.5 M NaOH or HCl solutions. Then, by a strong magnet, suspended magnetic nanoparticles were deposited at the bottom of the beaker and isolated from their suspension and after that the suspension solution became clear. Duplicate adsorption tests were conducted, and results were reported. The isotherm models of Freundlich and Langmuir were used to fit the experimental adsorption equilibrium data of fluoride

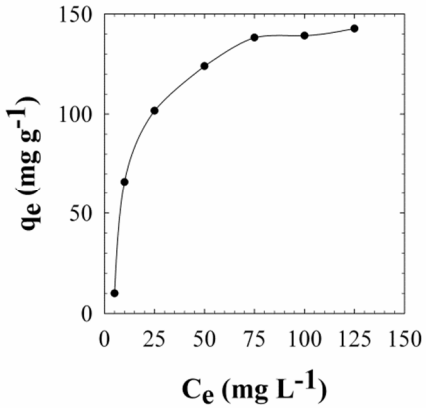

Fig. 9. Effect of initial fluoride ion concentration on its adsorption, adsorbent dose 1 mg mL^{-1}, 25 °C pH 2.5 and contact time 1 h.

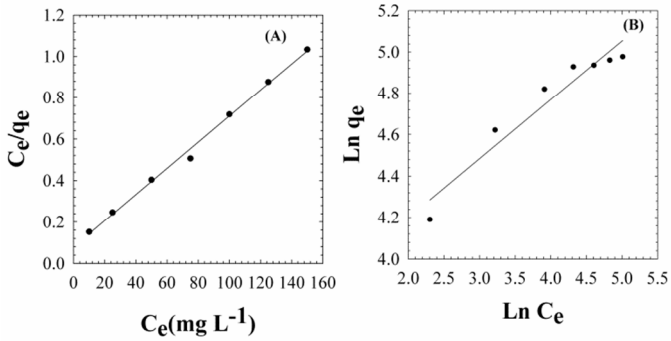

Fig. 10. The isotherm models of Freundlich **(A)** and Langmuir **(B)** used to fit the experimental adsorption equilibrium data of fluoride on magnetic adsorbents. Adsorbent dose 1 mg mL^{-1}, temperature 25 °C pH 2.5 and contact time 1 h.

on magnetic adsorbents. These results were fitted to the isotherm models which are represented in Table 2. Figs. 10A and B, and Table 2 show that the Langmuir model gave a better fit to the experimental data than Freundlich isotherm based on the values of regression coefficients (R^2). The maximum adsorption capacity of Fe_3O_4@ZrO_2 MNPs calculated from the linear form of Langmuir model was 158.6 mg g^{-1} (inset of Fig. 10A). The experimentally determined uptake capacity (145.2 mg L^{-1}) was found to be comparable with that obtained from the analysis of the Langmuir plot (158.6 mg L^{-1}), confirming that the interaction between the sorbate and the sorbent is through chemical bonding.

To the best of our knowledge, the as-prepared Fe_3O_4@ZrO_2 MNPs nanosorbent had a much higher adsorption capacity and comparable magnetization than that of the other magnetic adsorbents reported previously (Table 3). A comparison of the fluoride sorption capacities of different magnetic sorbents reported in the literature, along with the Fe_3O_4@ZrO_2 MNPs nanosorbent, is given in Table 3. It can be seen from this that on comparison, the fluoride sorption capacity of the Fe_3O_4@ZrO_2 MNPs nanosorbent is significantly higher than the other sorbents listed in Table 3. The higher fluoride sorption capacity of the Fe_3O_4@ZrO_2 MNPs is due to the availability of the positive charges on the surface for neutralization with fluoride ions. The superior adsorption capacity of the Fe_3O_4@ZrO_2 MNPs for fluoride indicates that it could be a potential candidate for treatment of industrial effluent with high-fluoride contents, not only due to its high adsorption capacity but also the ease of separation, which can help overcome difficulties in cases in which the polluted water contains solid suspensions.

3.6. Kinetic studies

The kinetics of sorption is one of the important parameters for designing any sorbent system. The time-dependent reactions of adsorption were carried out by agitation with vigorous stirring using a non magnetic stirrer at 25±1 ◦C and at a pH of 2.5, adsorbent dose of 1 mg mL^{-1} and fluoride concentration (25, 50 and 100 mg L^{-1}) in a water bath at some fixed temperatures (25, 35 and 50 ˚C). As can be seen, the fluoride adsorption was initially rapid up to 10 min, and after that time the adsorption percent increased only by about 10 %. It is observed that the time required to reach equilibrium was about 60 min. Therefore, an optimum shaking time of 60 min was chosen in the subsequent adsorption tests. To further quantify the changes of fluoride adsorption with time on the Fe_3O_4@ZrO_2 MNPs, the pseudo-first-order and pseudo-second-order kinetic models were used to simulate the kinetics. The pseudo-second-order model fits better based on the R^2 values (Fig. 11 and Table 4). The equilibrium adsorption capacities (q_e) were calculated as 102.38, 128.05, and 143.14 mg g^{-1} when the initial fluoride concentrations were 25, 50, and 100 mg L^{-1}, respectively. The value of $q_{e,cal}$ was in agreement with $q_{e,exp}$ based on pseudo-second-order model (Table 4).

In addition, the time-dependent adsorption kinetics studies of the Fe_3O_4@ZrO_2 MNPs were conducted at three different temperatures and analyzed using pseudo-second-order kinetic equations. As shown in Fig. 12 and Table 5, the initial adsorption rate h_0 and equilibrium adsorption capacity $q_{e,exp}$ values all increased with the increase of temperature from 25 to 50 ˚C, which suggested that the increase of temperature is beneficial for fluoride adsorption on the adsorbent. The increase in adsorption capacity and rate of fluoride adsorption with increasing temperature is relevant to the endothermic nature of fluoride adsorption on the magnetic adsorbents [39]. Finally, this suggests that the process was a pseudo-second-order reaction, thus, the kinetics of the fluoride sorption was governed by the binding sites on the composite as well as the fluoride concentration in the aqueous phase adjacent to the surface of the sorbent, leading to fast pseudo second order kinetics. In addition, the applicability of the pseudo-second-order model supports the results obtained from the Langmuir isotherm suggesting that the interaction of fluoride is via chemisorption and it is the rate determining step.

Table 2. Freundlich and Langmuir isotherms for fluoride ion adsorption onto the Fe_3O_4@ZrO_2 MNPs.

Isotherm model	Langmuir: $\frac{C_e}{q_e} = \frac{C_e}{q_m} + \frac{1}{q_m k_l}$			Freundlich: Ln q_e= Ln K_f + 1/n ln C_e		
Parameters	q_m (mg g^{-1})	K_1 (L mg^{-1})	R^2	K_F ($mg^{1-(1/n)}L^{1/n}g^{-1}$)	n	R^2
	158.6	0.079	0.996	37.7185	3.51	0.932

Ce is equilibrium concentration (mg L^{-1}), q_e is the amount adsorbed at equilibrium condition (mg g^{-1}), 1/n and K_f are isotherm constants. Experimental conditions: pH 2.5, adsorbent dose 1 g/L, 25°C,

Table 3. Comparison of the fluoride loading capacities and magnetization property of various magnetic adsorbents

Type of sorbent	Adsorption capacity (mg F^- g^{-1})	Magnetization property (emu g^{-1})	Ref.
Zr–polyacrylamide magnetic nanocomposite	124.5	4.5	[40]
Polypyrrole/Fe_3O_4 magnetic nanocomposite	22.31	NR*	[41]
ZrO_2/SiO_2/Fe_3O_4	14.7	7.1	[42]
Aluminum-type super paramagnetic adsorbents	38	8.7	[43]
Magnetic chitosan	23.98	NR	[44]
Iron oxide-hydroxide nanoparticles	1.66	16	[45]
Sulfate-doped Fe_3O_4/Al_2O_3 nanoparticles	70.4	NR	[46]
Fe_3O_4@$Al(OH)_3$ magnetic nanoparticles	88.48	17.9	[36]
Fe_3O_4@ZrO_2 MNPs	145.2	10.04	This work

NR; Not reported

RSC Advances

RSC Publishing

Paper

3.7. Thermodynamic parameters

The thermodynamic parameters for the adsorption process were calculated using the following relations:

$$\text{Log}\,(q_e/C_e) = \Delta S^0/2.303R - (\Delta H^0/2.303R)\ 1/T$$

$$\Delta G^0 = \Delta H^0 - T\Delta S^0$$

Where q_e/C_e is the adsorption affinity; ΔG^0, ΔH^0 and ΔS^0 are the change in free energy, enthalpy, and entropy, under standard states, respectively. The thermodynamic parameters were computed from the plot of $\log(q_e/C_e)$ versus 1/T for an initial fluoride concentration of 100 mgL^{-1}. The calculated value of ΔH^0 for $Fe_3O_4@ZrO_2$ MNPs was 25.02 kJ mol^{-1}, which definitely verify the endothermic nature of the fluoride adsorption process. The ΔS^0 obtained was 3.76 J mol^{-1} K^{-1}.

Using the values of ΔH^0 and ΔS^0, the ΔG^0 values have been calculated by mentioned equations and shown in Table 6, which indicated the adsorption of fluoride was spontaneous and the spontaneity of the process was enhanced with increasing temperature.

3.8. Effect of Interferences

Potable water commonly contains some anions which most important of them are chloride, sulfate, bicarbonate and nitrate [47] and as a result, these ions compete with fluoride ions for the active sites on the MNP surface. To study of the effect of these ions on the uptake of fluoride, the sorbent was equilibrated with a solution containing a binary mixture of fluoride and one of the competing ions. The variation in the defluoridation capacity of the $Fe_3O_4@ZrO_2$ MNPs in the presence of co-anions viz., Cl^-, SO_4^{2-}, NO_3^- and HCO_3^-, studied with a variable initial concentration of ions, and a fixed fluoride concentration of 50 mg L^{-1}.

The results indicated that sulfate ion had a little interference upon fluoride removal when their concentrations were equal or multiples of the concentration of fluoride. The presence of HCO_3^- significantly affected the fluoride removal. HCO_3^- ion is hydrolyzed in solution, leading to the increase of pH value. As a result, more hydroxyl ions would compete with fluoride on the active adsorption sites [48], which resulted in the decrease of adsorption capacity of the $Fe_3O_4@ZrO_2$ MNPs for fluoride. This result was in agreement with observation by Wang et al. [38]. Furthermore, the difference in the fluoride equilibrium loadings between single-component and multiple-component solutions is negligible. This demonstrates that $Fe_3O_4@ZrO_2$ MNPs have a considerable selectivity for fluoride which allows its preferred sorption from multicomponent systems.

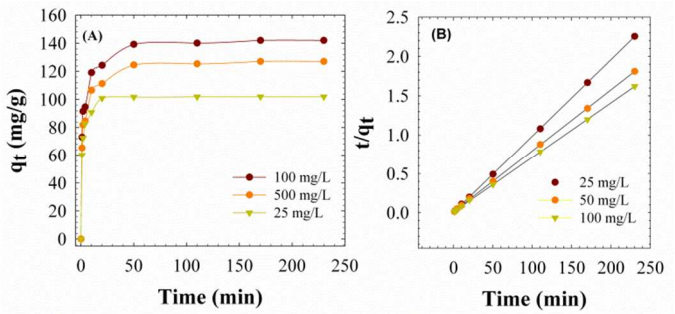

Fig 11. (A) Adsorption kinetic curves of fluoride adsorption on the $Fe_3O_4@ZrO_2$ (2:5) MNPs with different initial fluoride concentration. Adsorbent dose: 1 mg mL^{-1}, 25 ˚C, pH 2.5. **(B)** Pseudo-second-order kinetic plots for the adsorption of fluoride on the $Fe_3O_4@ZrO_2$ (2:5) MNPs at three different concentrations.

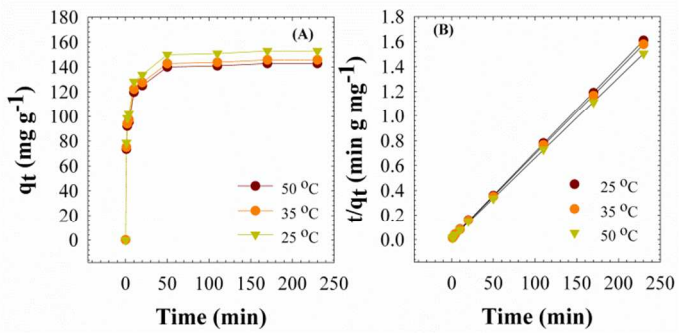

Fig 12. (A) Adsorption kinetic curves of fluoride adsorption on the $Fe_3O_4@ZrO_2$ (2:5) MNPs at different temperatures. **(B)** Pseudo-second order model for fluoride removal by the $Fe_3O_4@ZrO_2$ (2:5) MNPs at different temperatures. Adsorbent dose: 1 mg mL^{-1}, 25 ˚C, pH 2.5

In contact with water the surface of metal oxides undergoes a proteolytic reaction and, therefore, is covered with hydroxyl groups (see scheme 1). The amphoteric behaviour of the $Fe_3O_4@ZrO_2$ MNPs surface can be explained by the Brønsted–Lowry acid–base theory, which shows that the surface charge is strongly dependent on the solution pH. Generally, the protonated surface is predominant at pH value < pH_{PZC} and the deprotonated surface is predominant at pH value > pH_{PZC}, i.e. pH_{PZC} as 5.5 in this work.

3.9. Mechanism of fluoride adsorption

Table 4. Kinetic parameters of fluoride adsorption onto the $Fe_3O_4@ZrO_2$ (2:5) MNPs

Equation		First-order kinetics: $\ln(q_e-q_t)=\ln q_e-k_1t$			Second-order kinetics: $\frac{t}{q_t}=\frac{1}{k_2q_e^2}+\frac{t}{q_e}$		
C_0 (mg L^{-1})	$q_{e.exp}$ (mg g^{-1})	k_1 (min^{-1})	$q_{e.cal}$ (mg g^{-1})	R^2	k_2 (g (mg min)$^{-1}$)	$q_{e.cal}$ (mg g^{-1})	R^2
25	101.7	18.75×10^{-2}	57.30	0.785	1.34×10^{-2}	102.38	0.999
50	123.9	9.62×10^{-2}	67.29	0.796	4.35×10^{-3}	128.05	0.999
100	139.2	9.41×10^{-2}	75.87	0.791	3.89×10^{-3}	143.14	0.999

q_e and q_t are the amounts of fluoride ion adsorbed by MNPs at equilibrium and any time t, respectively. k_1 is the equilibrium rate constant of adsorption and t is the constant time.

RSC Advances RSC Publishing

Paper

As a consequence, the sorption of fluoride can simply be expressed as a ligand exchange or surface complexation as showed in scheme 1.

The sorption of fluoride is accompanied with the release of hydroxyl ions (OH^-); therefore, there is a favourable sorption at the pH < pH_{PZC}. If the pH value is higher than 5.5 (equal to pH_{PZC}), the surface becomes predominantly negatively charged. Thus sorption of anions decreases. The fluoride-loaded on Fe_3O_4@ZrO_2 MNPs can be regenerated by reversing adsorption reactions in scheme 1. Eventually, the ability of fluoride sorption can be reachieved by re-protonation of the Fe_3O_4@ZrO_2 MNPs surface according to scheme 1. Finally, fluoride sorption tests with the regenerated sorbent showed no decrease in the sorption capacity of the sorbent for 8 cycles but after the 8th cycle the kinetic of desorption become slower, thus the results indicate that the Fe_3O_4@ZrO_2 MNPs sorbent is reusable.

3.10. Fluoride removal from real samples

In order to investigate the removal performance of the Fe_3O_4@ZrO_2 MNPs in high fluoride contaminated waters, we added the standard stock solutions of fluoride, 1.0, 5.0, and 10.0 mg L^{-1}, into tap water sample solutions. The results obtained by applying Fe_3O_4@ZrO_2 MNPs for recovery tests of fluoride are shown in Table 7. Experimental results demonstrated that the water samples with a high fluoride concentration could be decreased to below the guideline limit regulated by the WHO by using adsorbent dosage of 0.25 mg ml^{-1} at pH 2.5 within 60 min. The results demonstrated validity of the method and potential applicability of Fe_3O_4@ZrO_2 MNPs for defluoridation of high levels fluoride in real samples.

Compared to previous defluoridation methods, the attractive merits of our method were three-fold: (a) high adsorption capacity and high selective affinity toward fluoride. Sorbents have higher surface areas and shorter diffusion route and the ZrO_2 surface layer of Fe_3O_4@ZrO_2 MNPs possess specific affinity toward fluoride, therefore, satisfactory results can be achieved by using less amount sorbents than traditional micron-size particle sorbents. (b) Rapid defluoridation treatment. The superparamagnetic and strong magnetization properties of the Fe_3O_4@ZrO_2 MNPs are favourable for MCT. The treatment process avoids the time-consuming adsorbent bed passing and exhibits great potential in treatment of large volume real water samples. (c) Easy preparation, which can meet the need of practical application for treatment of large volume high-fluoride contaminated water.

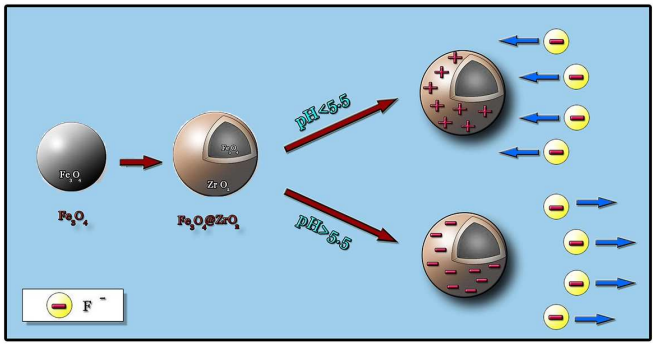

Scheme 1. Proposed mechanism for fluoride removal by using Fe_3O_4@ZrO_2 MNPs

4. Conclusions

Table 5. Fluoride adsorption pseudo-second-order kinetic constants for Fe_3O_4@ZrO_2 MNPs at different temperatures with initial fluoride concentration of 50 mg L^{-1}.

Initial temp. (˚C)	$q_{e.exp}$ (mg g^{-1})	*h_o (mg (g min)$^{-1}$)	k_2 (g (mg min)$^{-1}$)	$q_{e.cal}$ (mg g^{-1})	R^2
25	140.0	80.28	3.87×10^{-3}	144.0	0.999
35	142.8	81.88	3.80×10^{-3}	146.9	0.999
40	149.8	85.90	3.62×10^{-3}	154.1	0.999

*The initial sorption rate, h_0 (mg (g min)$^{-1}$) can be defined as: $h_0=k_2q_e^2$ ($t\rightarrow 0$)

Table 6. Thermodynamic parameters for the adsorption process of fluoride by using Fe_3O_4@ZrO_2 MNPs

ΔH°(kJ mol^{-1})	ΔS°(J mol^{-1} K^{-1})	R^2	Temperature	25°C	40°C	50°C
25.02	3.76	0.99	ΔG° (kJ mol^{-1})	23.90	23.86	23.81

Table 7. The results obtained for recovery tests of fluoride, from spiked standard samples in tap water, by applying Fe_3O_4@ZrO_2 MNPs

Water sample	Added F^- (mg L^{-1})	Remained F^- After treatment (mg L^{-1})	Recovery
Tap water	5.0	0.1±0.1	98.0%
	10.0	0.1±0.1	99.0%
	20.0	0.3±0.1	98.5%

Acknowledgments

The authors gratefully acknowledge the NSTRI providing facilities for this work. And also, the financial support of the Iran National Science Foundation (INSF) are gratefully acknowledged (project 89001654).

[a] Material Research School, NSTRI, Isfahan 81465-1589, I.R. IRAN.
[b] Islamic Azad University, Shahreza Branch, Shahreza, I.R. IRAN.
Corresponding author. E-mail address: mjmo123@yahoo.com (Dr. M. Bagherzadeh).

Notes and references

Electronic Supplementary Information (ESI) available: [calibration curve obtained from UV-Visible and zeta potential mesurment]. See DOI: 10.1039/b000000x/

[1] M. Faraji, Y. Yamini, M. Rezaee, *J. Iran. Chem. Soc.,* 2010, **7**, 1.
[2] A.H. Lu, E.L. Salabas, F. Sch_th, *Angew. Chem. Int. Ed.* 2007, **46**, 1222.
[3] M. Ajmal, M. Siddiq, N. Aktas, N. Sahiner, *RSC Adv*. 2015, **5**, 43873.
[4] H. Gu, S.B. Rapole, J. Sharma, Y. Huang, D. Cao, H.A. Colorado, Z. Luo, N. Haldolaarachchige, D.P. Young, B. Walters, S. Wei, Z. Guo*, RSC Adv*. 2012, **2**, 11007.
[5] X. Guan, J. Chang, Y. Chen, H. Fan, *RSC Adv.* 2015,**5**, 50126.
[6] L. Li, M. Xu, M. Chubik, M. Chubik, A. Gromov, G. Wei, W. Han, *RSC Adv.* 2015,**5**, 41611.
[7] X.Q. Xu, C.H. Deng, M.X. Gao, W.J. Yu; P.Y. Yang, X.M. Zhang, *Adv. Mater.* 2006, **18**, 3289.
[8] C.-T. Chen, Y.-C. Chen, *Anal. Chem*. 2005, **77**, 5912.
[9] J.C. Liu, P.J. Tsai, Y.C. Lee, Y.C. Chen, *Anal. Chem.* 2008, **80**, 5425.
[10] C.Y. Lo, W.Y. Chen, C.T. Chen, Y.C. Chen, *J. Proteome Res.* 2007, **6**, 887.
[11] S. Meenakshi, C.S. Sundaram, R. Sukumar, *J. Hazard. Mater.* 2008, **153**, 164–172.
[12] S. Tokunaga, M.J. Haron, S.A. Wasay, K.F. Wong, K. Laosangthum, A. Uchiumi, *Int. J. Environ. Studies* 1995, **48**, 17.
[13] X.M. Dou, D. Mohan, C.U. Pittman, S. Yang, *Chem. Eng. J.* 2012, **198**, 236.
[14] C.Y. Lo, W.Y. Chen, C.T. Chen, Y.C. Chen, *J. Proteome Res.* 2007, **6**, 887.
[15] Y. Li, T. Leng, H. Lin, C. Deng, X. Xu, N. Yao, P. Yang, X. Zhang, *J. Proteome Res.* 2007, **6**, 4498.
[16] B.D. Turner, P. Binning, S.L.S. Stipp, *Environ. Sci. Technol.* 2005, **39**, 9561.
[17] WHP Guideline for Drinking Water Quality: Incorporating First Addendum Recommendations, vol. 1, 3rd ed., WHO, 20 Avenue Appia, 1211 Geneva 27, Switzerland, 2006, pp. 375–376.
[18] M. Yang, Y. Zhang, B. Shao, R. Qi, H. Myoga, *J. Environ. Eng.* 2001, **127** (10), 902.
[19] C. Castel, M. Schweizer, M.O. Simonnot, M. Sardin, *Chem. Eng. Sci.* 2000, **55**, 3341.
[20] K. Biswas, S.K. Saha, U.C. Ghosh, *Ind. Eng. Chem. Res.* 2007, **46**, 5346.
[21] X.L. Zhao, Y.L. Shi, Y.Q. Cai, S.F. Mou, *Environ. Sci. Technol.* 2008, **1139**, 178.
[22] M. Bagherzadeh, S. Ansari, F. Riahi, A. Farahbakhsh, *Inter. J. Electrochem.* 2013, 1.
[23] P. Pommerenk, G.C. Schafran, *Environ. Sci. Technol.* 2005, **39**, 6429.
[24] R.K. Shervedani, M. Bagherzadeh, *Sens. Actuat. B* 2009, **139**, 657.
[25] Huang, P.M. and M.L. Jackson. 1967. Fluorine Determination in Minerals and Rocks. *American Mineralogist* 52:1503-1507.
[26] K. Kuratani, M. Uemura, M. Mizuhata, A. Kajinami, S. Deki, *J. Am. Ceram. Soc.*, 2005, **88**, 2923.
[27] S. Ardizzone, C. L. Bianchi, *Appl. Surf. Sci.*, 1999, **152**, 63.
[28] C. D. Wagner, W. M. Riggs, M. E. Davis, S. F. Moulder, and G. E. Muilenberg, Handbook of X-Ray Photoelectron Spectroscopy, Perkin-Elmer, New York, NY, USA, 1996.
[29] P. Ragupathy, D. H. Park, G. Campet, H. N. Vasan, S. J. Hwang, J. H. Choy, N. Munichandraiah, *J. Phys. Chem. C,* 2009, **113**, 6303.
[30] N. D. Kim, H. J. Yun, I. Nam, J. Yi, *J. Mater. Chem.*, 2011, **21**, 15885.
[31] D.B. Cullity, S.R. Stock, Elements of X-ray Diffraction, Prentice Hall, New Jersey, 2001.
[32] X.Q. Xu, C.H. Deng, M.X. Gao, W.J. Yu, P.Y. Yang, X.M. Zhang, *Adv. Mater.* 2006, **18**, 3289.
[33] S. Zhou, G. Garnweitner, M. Niederberger, M. Antonietti *Langmuir* 2007**, 23***,* 9178.
[34] M. Bagherzadeh, M. Pirmoradian, F. Riahi, *Electrochim. Acta* 2014, **115**, 573.
[35] C.-F. Chang, C.-Y. Chang, T.-L. Hsu, *Collo. Surf. A Phys. Eng. Aspects* 2008, **327**, 64.
[36] X.L. Zhao, J.M. Wang, F.C. Wu, T. Wang, Y.Q. Cai, Y.L. Shi, G.B. Jiang, *J. Hazard. Mater.* 2010, **173**, 102.
[37] X. Wu, Y. Zhang, X. Dou, M. Yang, *Chemosphere* 2007, **69** 1758.
[38] J. Wanga, W. Xu, L. Chen, Y. Jia, L. Wanga, X.-J. Huang, J. Liu, *Chem. Engin. J.* 2013, **231**, 198.
[39] K. Biswas, S.K. Saha, U.C. Ghosh, *Ind. Eng. Chem. Res.* 2007, **46**, 5346.
[40] N. Thakur, S.A. Kumar, H. Parab, A.K. Pandey, P. Bhatt, S.D. Kumar, A.V.R. Reddy, *RSC Adv*. 2014, **4**, 10350.
[41] M. Bhaumik, T.Y. Leswifi, A. Maity, V.V. Srinivasu, M.S. Onyango, *J. Hazard. Mater.* 2011, **186**, 150.
[42] C.-F. Chang, C.-Y. Chang, T.-L. Hsu, *Desalination*, 2011, **279**, 375.
[43] C.–F. Chang, P.-H. Lin, W. Holl, *Colloids Surf. A* 2006, **280**, 194.
[44] W. Ma, F.-Q. Ya, M. Han, R. Wang, *J. Hazard. Mater.* 2007, **143**, 296.
[45] P. K. Raul, R. R. Devi, I. M. Umlong, S. Banerjee, L. Singh M. Purkait, *J. Nanosci. Nanotechnol*. 2012, **12**, 3922.
[46] L. Chai, Y. Wang, N. Zhao, W. Yang, X. You, *Water Res.* 2013, **47**, 4040.
[47] E.J. Reardon, Y.X. Wang, *Environ. Sci. Technol.* 2000, **34**, 3247.
[48] L. Lv, J. He, M. Wei, D.G. Evans, X. Duan, *J. Hazard. Mater. B* 2006, **133**, 119.

